Design Study of Charge-Stripping Scheme of Heavy Ion Beams for HIAF-BRing

Jun-Jie Zhang[1,2], Zhi-You Xu[1,2], Jin-Quan Zhang[1], Wen-Wen Ge[1], Liang-Ting Sun[1,2] and Huan-Yu Zhao[1,2,*]

[1]Institute of Modern Physics, Chinese Academy of Sciences, Lanzhou 730000, China

[2]School of Nuclear Science and Technology, University of Chinese Academy of Sciences, Beijing 100049, China

Abstract

Charge strippers play an essential role in heavy-ion accelerators by stripping the projectile ions to higher charge states to enhance the acceleration efficiency downstream of the stripper. In the high-energy mode of the booster ring (BRing) of the high-intensity heavy-ion accelerator facility, the pre-accelerated ions from the iLinac will be stripped by a carbon foil to higher charge states and then injected into the BRing. The key parameters of the stripper and stripped ions were calculated, and the influence of stripping on the beam quality was discussed. To get high stripping efficiencies, the foil thicknesses and resultant charge state distributions for the typical ions were determined by the code ETACHA. The equilibrium thickness was obtained for the U beam, while the stripper thicknesses for the Xe and Kr beams were determined based on a compromise between the stripped charge states and the stripping efficiency. The energy loss, energy straggling, and emittance growth due to stripping have a non-negligible impact on the transport of the stripped beams and the injection of the ring. Therefore, these parameters were simulated by GEANT4. In addition, the foil's temperature evolution, which greatly affects the foil lifetime, was simulated by ANSYS. The maximum temperature of the foil bombarded by the U and Xe beams with the nominal parameters will exceed the safe value in terms of the impact of evaporation on the foil's lifetime. Given the foil temperature constraint, the highest tolerable beam intensity and the injected ion number into the ring were derived for different beam sizes. The results of this paper will present important reference data for the optimization design and commissioning of the beamline and injection to the BRing for the stripped ions.

Keywords: high-intensity heavy-ion accelerator facility; charge stripper; energy spread; thermal analysis; emittance growth; injection turns

1. Introduction

High-intensity heavy-ion accelerator facility (HIAF) [1] [2] is a next-generation storage-ring-based heavy-ion facility proposed by the Institute of Modern Physics (IMP). The major scientific goals of HIAF are to explore the hitherto unknown territories in the nuclear chart, study exotic nuclear structures, synthesize super-heavy nuclides and elements, understand the origin of heavy elements in the universe, and develop novel heavy-ion applications in space and material sciences [3] [4]. Since 2016, HIAF has been under design and construction [5]. HIAF comprises a 45-GHz superconducting electron cyclotron resonance (ECR) ion source [6]–[8], a superconducting ion Linac (iLinac) [9]–[11], a booster ring (BRing) [12]–[14], a high-energy radioactive beamline (high energy fragment separator (HFRS)) [15], a storage ring (SRing) [16] [17], and several experimental terminals. The ions produced by the ion source will be accelerated by the iLinac to a particular energy, depending on the charge-to-mass ratio of the ions, and then injected into the BRing, where the ions will be accumulated and further accelerated to high energy. To meet the requirements of the different experiments, the BRing can provide very intense heavy ion beams with reasonable energies or ion beams with higher energies at the expense of beam intensities. Taking the ion of uranium as an example, over 1.0×10^{11} U^{35+} ions can be stored in the BRing, and the highest energy would be 835 MeV/u, or the energy of 2.6 GeV/u could be achieved while the intensity would be much lower [5].

* Corresponding author.
E-mail address: zhaohy@impcas.ac.cn (H. Y. Zhao)

In the latter case, the ions need stripping to higher charge states before they are injected into the BRing such that higher acceleration efficiency can be gained in the ring.

Charge strippers are widely utilized in heavy ion accelerator facilities at different energy stages to enhance the acceleration efficiencies downstream of the strippers. The unprecedented high power of the ion beams from state-of-the-art accelerator facilities, such as the RIKEN RI Beam Factory (RIBF, Japan), the Facility for Antiproton and Ion Research (FAIR, Germany), the Facility for Rare Isotope Beams (FRIB, U.S.A.) and HIAF, etc., presents a significant challenge to the strippers. To accommodate to the different ion beam conditions, various strippers are employed at these facilities. For example, there are two strippers at RIBF: one is a helium gas stripper to strip U^{35+} to U^{64+} at the energy of 10.8 MeV/u [18] [19], and the other is a rotating highly oriented graphite sheet to strip U^{64+} to U^{86+} at 51 MeV/u, which performs excellently in terms of the lifetime owing to its superior thermal diffusion and thermal conduction properties [20] [21]. To meet the high-intensity heavy-ion requirements for the FAIR project, a high-density fast pulsed hydrogen-gas cell stripper has been developed to strip 1.4 MeV/u U^{4+} ions with a current intensity up to 7.6 emA and the pulse duration of 100 μs [22]–[24]. Owing to the pulsed gas cell synchronized with the ion beams, a high stripper density was achieved while the gas load was reduced significantly, resulting in an increased stripping efficiency compared with the previous nitrogen gas jet operated in continuous mode. Considering the high average thermal power deposited by the continuous high-power ion beams at FRIB, a windowless liquid lithium free-jet stripper has been developed in collaboration with Argonne National Laboratory (ANL). The hydrodynamic stability of the lithium jet was obtained with a flow velocity of 50 m/s, which also enables the removal of the extraordinarily high power [25] [26]. As for HIAF, the charge stripper should meet the requirements of stripping various ion species from H_3^+ to $^{238}U^{35+}$: heavy ions should be stripped to sufficiently high charge states, whereas H_3^+ ions need to be stripped to protons efficiently. Owing to the density effect [27] [28], the average charge state resulting from a carbon-foil stripper is higher than that from a gas stripper. Moreover, stripping is only needed for the pulsed beams with moderate beam intensity and low duty cycle (0.1% based on 1-ms beam pulse duration and 1-Hz repetition rate, or even lower (see the discussion in Section 5.2), which means the average beam intensity is low. Therefore, a carbon foil stripper is chosen as the baseline design at this stage for HIAF-BRing.

Here, some key issues concerning the HIAF's charge stripper, such as the charge state distributions after the stripper, the lifetime issues due to the thermal load, the emittance growth due to the stripping process, and the resultant effect on the ion number injected into the ring, will be presented and discussed.

2. Charge Stripper of HIAF-BRing

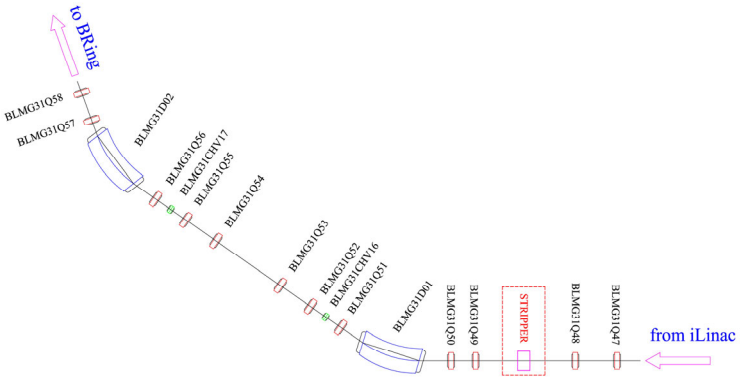

Fig. 1. Location of charge stripper on beamline to BRing.

As illustrated in Fig. 1, the carbon foil stripper will be located at the injection line to the BRing. The ion beams accelerated by the iLinac will be stripped here if needed. The typical beam parameters from the iLinac are presented in Table 1. To minimize the emittance growth and beam loss caused by the enhanced space charge forces after stripping, the ions after the stripper will be separated immediately by the following dipole magnets.

Ion species	Energy (MeV/u)	Current intensity (emA)	Pulse duration (ms)	Repetition frequency (Hz)	Emittance-geometric (π mm·mrad)[1]	Moment spread
$^{78}Kr^{19+}$	27	1	1	1	6.5	±0.2%
$^{129}Xe^{27+}$	30	1				
$^{238}U^{35+}$	17	1				

Table 1 Typical ion beam parameters from iLinac

Compared with protons, the energy loss per ion per unit length in the stripper is much higher for heavy ions, especially for U ions, which brings a great challenge to the stripper in terms of its lifetime. In addition, the charge state distributions after stripping and the stripping efficiencies are of the most concern. In some cases, like for Xe and Kr ions, these two factors conflict, and a compromise must be made by choosing appropriate foil thickness, as seen in Section 3.

3. Charge state distributions after stripping

During the passage of the projectile ions through the stripper, the competition between electron loss and electron capture processes results in the evolution of the charge states of the ions. The cross sections of electron loss and electron capture converge gradually with the increasing charge state of the ions, i.e., the increasing passage thickness of the ions, and thus, the charge state distribution of the ions finally gets to equilibrium. The average charge state that can be obtained by stripping depends on the energy, the atomic number of the projectile ion, and the atomic number of the stripper as well. When a charge stripper is utilized, the equilibrium thickness must be determined beforehand such that high stripping efficiency can be achieved and extra emittance growth, energy loss, and energy straggling caused by unnecessary stripper thickness can be avoided. Dedicated codes such as ETACHA, GLOBAL, etc. can calculate equilibrium thicknesses and charge state distributions. The ETACHA code is appropriate for simulating the charge state evolution of the ions in a non-relativistic energy range crossing a solid or gas stripper, with the density effects and the shell effects taken into account [29] [30].

The charge state distributions of the typical ions after stripping calculated by the ETACHA code are illustrated in Fig. 2, which illustrates that the fraction of 50%, 19.5%, and 26.7% can be reached for Kr^{34+}, Xe^{50+}, and U^{79+} ions with the carbon foil thicknesses of 0.675, 0.85, and 1.0 mg/cm^2, respectively. Among these three ion species, the equilibrium charge state is only achieved for U, which agrees well with the mean charge state predicted by Baron's formula [31]. For the Kr and Xe ions, the most-populated charge states and the average charge states can be further increased by increasing the thicknesses of the strippers. However, the electron loss cross sections for the last two L-shell electrons, as in the case of Xe, and those for the K-shell electrons in the case of Kr, are much smaller than those for the outer electrons, which means that much thicker strippers than the present ones are required to get the equilibrium charge states while the stripping efficiency will decrease considerably. More importantly, the energy loss, energy straggling, and emittance growth will consequently increase (the influence of the stripper thickness on those parameters will be discussed below). Therefore, we choose the thinner thicknesses to get higher stripping efficiency and reasonable beam quality on a tradeoff of slightly lower charge states of the stripped ions. In the following part of this paper, all the calculations were based on the stripper thicknesses presented in this section, i.e., 0.675, 0.85, and 1.0 mg/cm^2 for Kr, Xe, and U ions, respectively.

[1] The emittances presented in this paper are all geometric ones, which will not clarified specifically in the following part.

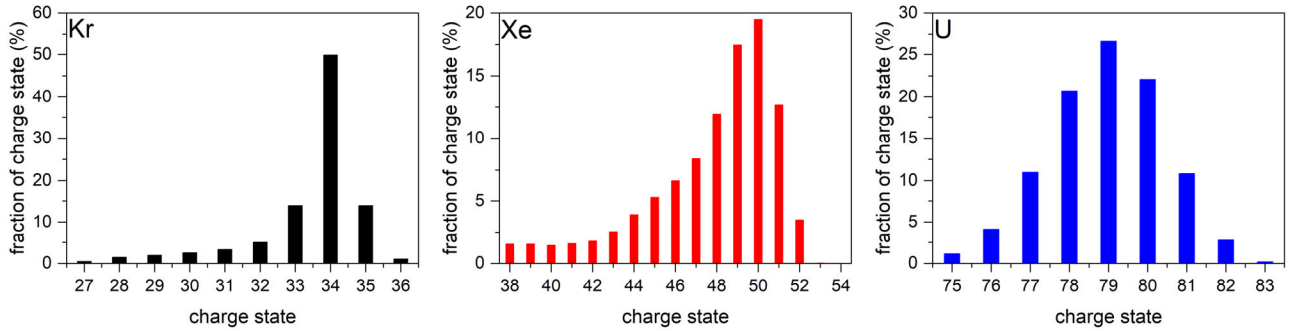

Fig. 2. Charge state distributions of Kr, Xe, and U ions after stripping with carbon foil thicknesses of 0.675, 0.85, and 1.0 mg/cm^2, respectively.

4. Energy losses and energy spreads due to stripping

Ions not only lose electrons but also lose energy while passing through strippers. When a stripper is utilized, the energy loss and, more accurately, the energy distribution function of the ions after the stripper need to be considered. Given the thickness of the stripper t_{foil}, the energy loss could be calculated roughly utilizing the following formula.

$$\Delta E = \left(\frac{dE}{dx}\right) t_{foil} \tag{1}$$

where ΔE is the energy loss during the stripping; $\frac{dE}{dx}$ is the stopping power at the input energy, and t_{foil} is the thickness of the stripper. This calculation is coarse. First, the change of the stopping power due to the change of the ion energy on the path of the ions through the stripper is ignored. Moreover, extra energy spread will be introduced and superimposed on the initial one. Neglecting the change of the stopping power will not bring appreciable error to the result because the change is minute. Taking U ions as an example, the stopping power of carbon is 113.1 MeV/(mg/cm^2) for 17 MeV/u U ions and 114 MeV/(mg/cm^2) for 16.55 MeV/u U ions, the energy of the U ions exiting the stripper. While the energy spread due to the stripping must be considered because it will influence the transport of the ions downstream of the stripper. The energy spread during the passage of ions through a stripper comes from intrinsic and extrinsic causes. The intrinsic energy-loss straggling is determined by the collision straggling, the stochastic fluctuations of the energy loss in atomic collisions with fixed charge states, and the charge-exchange straggling, the energy straggling caused by the stochastic variations of the ions' charge states when they traverse the foil [32]. And the extrinsic cause is the non-uniformity of the foil thickness.

To calculate the energy distributions of the ions after the stripper, the Monte Carlo calculations were carried out with the code GEANT4 [33] [34]. GEANT4 allows user-defined particle energy distributions and target thicknesses; thus, the initial energy distributions of the ions before stripping were utilized as the input parameters, and the non-uniform foil thicknesses. Carbon foils commonly have a deviation of ±5% from the nominal thicknesses, which was adopted in our calculations of the energy distributions. Fig. 3 presents the energy distributions of the typical ions after the strippers calculated by the code GEANT4. To validate the calculations of GEANT4, the results for monoenergetic ions traversing uniform foil calculated by GEANT4 were compared with those calculated by SRIM [35], a well-established program dedicated to calculating the stopping and range of ions in matter. The output energy and the energy straggling calculated by the two programs were consistent.

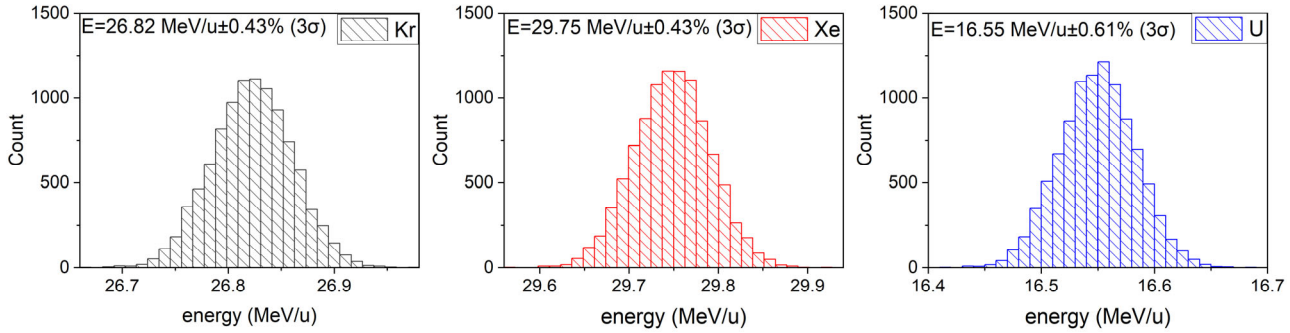

Fig. 3. Energy distributions of Kr, Xe, and U ions after traversing foil strippers of 0.675, 0.85, and 1 mg/cm^2, respectively (charge exchange straggling not included).

As illustrated in Fig. 3, the average energy of Kr, Xe, and U ions after stripping is 26.82, 29.75, and 16.55 MeV/u, respectively. The energy spread of the U beam is larger than that of the Kr and Xe beams, which is easy to understand. The energy spread introduced by the non-uniform foil thickness can be estimated with the following equation.

$$\sigma_{E-Thi.Dev.} = \sigma_{Thi.} t_{foil} \left(\frac{dE}{dx}\right) \tag{2}$$

where $\sigma_{E-Thi.Dev.}$ is the energy deviation caused by the non-uniform foil thickness, and $\sigma_{Thi.}$ is the deviation of the foil thickness. The foil thickness and the stopping power are larger for U ions than those for the two other ions, so the non-uniformity of the foil thickness has a more remarkable influence on the energy spread for U ions.

In the models of GEANT4 and SRIM, the projectile ions are treated with an effective charge, which means the charge exchange straggling is not considered during the calculations. It will lead to an underestimation of the final energy spread. To calculate the charge exchange straggling accurately, the cross sections for all relevant electronic transitions in the projectile all along its traveling path are needed. Much theoretical work [32] [36]–[38] has been elaborately conducted to deal with that. Here, we adopted Yang's empirical formula [39], widely utilized to calculate electronic energy loss straggling. Stemming from Bohr's classical formula, Yang et al. considered charge state fluctuations and other correlation effects and consequently developed the following empirical straggling formula.

$$\Omega_{Yang}^2 = \Omega_{Bohr}^2 \left[\gamma^2(Z_1, Z_2, v)\left(\frac{\Omega_{Chu}^2}{\Omega_{Bohr}^2}\right) + \left(\frac{\Delta\Omega_{Ion}^2}{\Omega_{Bohr}^2}\right)\right] \tag{3}$$

where $\gamma(Z_1,Z_2,v)$ is the effective charge factor of ions in matter, Ω_{Bohr} is the energy straggling based on Bohr's theory [40], and Ω_{Chu} and $\Delta\Omega_{Ion}$ are the straggling contributions due to Chu's theory [41] and correlation effect, respectively. A series of fitted constants are needed to calculate Yang's straggling with Equation 3. Table 2 lists Yang's straggling calculated with Equation 3 and those contributed by the initial energy spread and the foil's inhomogeneity. With all these contributions, the final energy spreads of the ions just exiting the stripper were calculated, as presented in Table 2. It implies that the energy spreads, including the contributions of charge exchange straggling, are higher than the values in Fig. 3 by 16% roughly.

Ion species	Contributions to final energy spread (σ-%)			Final energy spread (σ-%)
	Initial spread	Yang's energy straggling	Non-uniformity of thickness	
Kr	0.133	0.029	0.033	0.144
Xe	0.133	0.066	0.044	0.153
U	0.133	0.131	0.140	0.236

Table 2. Final energy spreads and sources contributing to them

5. Compromise between stripper temperature and emittance growth

5.1 Constraint on foil temperature

When a solid-state stripper is utilized, its lifetime is one of the main concerns. The lifetime of a foil stripper is mainly determined by accumulated radiation damage and evaporation of the foil. From the first adoption of solid-state strippers, researchers have been making efforts to estimate the lifetime of strippers quantitatively. Among them, Levedev drew a physical picture of carbon foils' failure under irradiation and derived the formulae to estimate the lifetime of carbon foils due to radiation damage [42]. Based on Levedev's theory, "stripper lifetime utility" was integrated into the program LISE++ since Version 8.3.6 [43], which utilizes Equation 15 in Ref. [42] to calculate the lifetime of carbon foils due to radiation damages. In the following updated versions, k_1's dependence on the atomic number of the projectile has been introduced to reproduce experimental data for projectiles in a wide region, and then Equation 15 in Ref. [42] has been transformed as follows

$$t = k_1(Z_1)K_d^{-\frac{5}{4}}\exp\left(-\frac{k_2}{T}\right), k_1(Z_1) = k_{10}\exp\left(-k_{11}Z_1\right) \tag{4}$$

where t is the foil lifetime dominated by the radiation damage; K_d is the rate of atom displacement, and its expression can be found in Ref. [42], Z_1 is the atomic number of the projectile; k_2 is a characteristic constant related to the foil material and its default value for carbon is 870, and the default values of k_{10} and k_{11} are 50 and -0.07, respectively. With the modification of k_1, the calculated results are in better agreement with the experimental results in a wide region (from Ne to U).

Compared with some semi-empirical treatments during the derivation of Equation 4, the calculation of the foil evaporation could be more accurate. Although the sublimation temperature of the carbon is approximately 3900 K, evaporation occurs for a carbon foil bombarded by intensive ion beams even if the temperature is much lower than 3900 K. The evaporation rate increases with the temperature as follows [44] [45]

$$\log_{10}(dm/dt) = \log_{10} P_{atm} - 0.5\log_{10} T - 2.187 \tag{5}$$

where dm/dt is the evaporation rate in (g/cm^2)/s; T is the temperature of the carbon foil in K; P_{atm} is the vapor pressure of carbon in the atmosphere and is also a function of T.

$$\log_{10} P_{atm} = -37.3(1000/T) + 8.16 \tag{6}$$

According to the research of *Lebedev et al.* [42], the failure of a carbon foil is dominated by irradiation damage at the temperature below 2500 K and by evaporation and sublimation at the temperature beyond 2500 K, in which case the lifetime of the carbon foil is generally only a few hours or even shorter. Here, we set a limit of 2200 K on the foil temperature, corresponding to a maximum evaporation rate of 10^{-3} (μg/cm^2)/s.

5.2 Non-stationary thermal analysis of foil bombarded by pulsed ion beams

To evaluate the lifetime of the stripper foil in terms of heating effect, the temperature evolution of the foil was calculated with the code Ansys with a non-stationary thermal model. The following equations can describe the heat conduction in the foil [46].

$$\frac{1}{\alpha c_p}\frac{\partial T}{\partial t} = \nabla^2 T + \frac{1}{kt_{foil}}[P - 2\sigma_0\varepsilon(T^4 - T_0^4)], \alpha = k/\rho c_p \text{ (m}^2\text{/s)} \tag{7}$$

where T is the temperature of the foil; T_0=295 K is the ambient temperature; t is the time; α is the thermal diffusivity of carbon; ρ=2000 kg/m^3 is the density of carbon; σ_0=5.67×10^{-8} W(m^{-2}·K^{-4}) is the Stefan–Boltzmann constant, ε is the emissivity of carbon and is set to 0.8 in the simulation; c_p and k are the specific heat capacity and heat conduction coefficient of carbon and are also functions of the temperature T [46].

$$c_p = 12.7 + 2.872T - 0.00145T^2 + 3.12\times10^{-7}T^3 - 2.38\times10^{-11}T^4 \text{ J/(kg·K)}$$

$$k = 241.54 - 0.241T + 1.088 \times 10^{-4}T^2 - 2.144 \times 10^{-8}T^3 + 1.531 \times 10^{-12}T^4 \text{ W/(m·K)} \quad (8)$$

P in Equation 6 represents the power density deposited in the foil by the pulsed ion beams and can be expressed as follows.

$$P = \frac{j}{q}\left(\frac{dE}{dx}\right) t_{foil} \text{ W/m}^2 \quad (9)$$

where j is the electrical current density, and q is the charge quantity of the incident ions, the product of the ion charge state and the elementary charge. Here, we assume the transverse beam distribution is 2-dimensional Gaussian.

$$j(x,y) = \frac{I}{2\pi\sigma_x\sigma_y} \exp\left(-\frac{(x-x_0)^2}{2\sigma_x^2}\right) \exp\left(-\frac{(y-y_0)^2}{2\sigma_y^2}\right) \text{ A/m}^2 \quad (10)$$

where I is the total beam intensity, x_0 and y_0 are the coordinates of the beam center on the carbon foil, and σ_x and σ_y are the rms beam spot size in the horizontal and vertical directions, respectively. In the simulation, the dependence of the stopping power $\left(\frac{dE}{dx}\right)$ on the energy was ignored because the energy loss of the beam is much lower compared with the incident energy, and the variation of the foil thickness with the temperature was not considered, either.

With the non-stationary model, the evolution of the foil temperature for the beam parameters listed in Table 1 (1-emA beam intensity in 1-ms pulse duration with the repetition frequency of 1 Hz) was simulated by the code Ansys. The values of σ_x and σ_y were set to 2.45 mm, which are the baseline design values for the injection beamline at the position of the stripper. The maximum foil temperature for U and Xe beams are 4188.3 and 2460.6 K, respectively, resulting in very short lifetimes of the strippers due to evaporation, which is unacceptable.

5.3 Synthesis of foil temperature, emittance growth, and number of injection turns

One important fact has been ignored in the preceding temperature calculation. In the simulation, we took the beam pulse duration of 1 ms. This value corresponds to the injection turns of 100 for the BRing [47] [48], derived based on the emittance of 5 π mm·mrad, i.e., for the unstripped ion beams[2]. Meanwhile, emittance growth is inevitable when an ion beam traverses a stripper owing to small-angle scattering of the projectile ions off the target atoms. Taking account of the emittance growth during stripping, the number of injection turns for stripped ion beams cannot achieve that for unstripped ion beams; hence, the beam pulse duration of 1 ms is unnecessarily long.

To determine the beam's appropriate pulse duration, the stripped beam's emittance needs to be known such that the number of injection turns could be estimated correspondingly. The emittance for the beam traversing foil can be calculated by the Monte Carlo codes, such as SRIM and GEANT4. Here, the GEANT4-10.06.p02 was utilized to calculate the emittance of the stripped ion beam. In Fig. 4, we present the simulated beam distributions in the horizontal/vertical phase space for the U beam just exiting the C-foil stripper of 1 mg/cm^2 calculated with GEANT4 and that for the beam just before the stripper.

As stated in Refs. 1 and 28, the two-plane painting injection scheme will be applied for the BRing, in which the number of injection turns can be estimated by the following empirical equation [49]–[51].

$$N_{inj-turn} = \alpha \frac{A_x A_y}{\varepsilon_x \varepsilon_y} \quad (11)$$

where A_x=200 π mm·mrad and A_y=100 π mm·mrad are the acceptances of the BRing in the horizontal and vertical phase spaces, respectively; ε_x and ε_y are the horizontal and vertical emittances (6 rms) of the beam, respectively, and α is the dilution factor, the value of which is in the range of 0.1–0.125 [51]. Here, the value of α is set as 0.125. Taking the emittance of 12 π mm·mrad for the stripped U beam into Equation 10, one can obtain the injection turn number of 18; hence, the beam pulse duration of 0.184 ms, corresponding to 18 revolution periods for the stripped U ions in the BRing, is long enough. The shortened beam pulse duration reduces the thermal load by one beam pulse and the consequent decrease of the maximum foil temperature to 1350.4 K, much lower than the temperature constraint, 2200 K. The beam pulse duration,

[2] It needs mentioning that 5 π mm·mrad is previous design value, which has been updated to 6.5 π mm·mrad as listed in Table 1.

even the nominal one-1 ms, is too short compared with the thermal diffusion in a carbon foil; hence, the energy deposited by the beam could be taken to be instantaneous. That is why the maximum temperature correlates directly with the beam pulse duration.

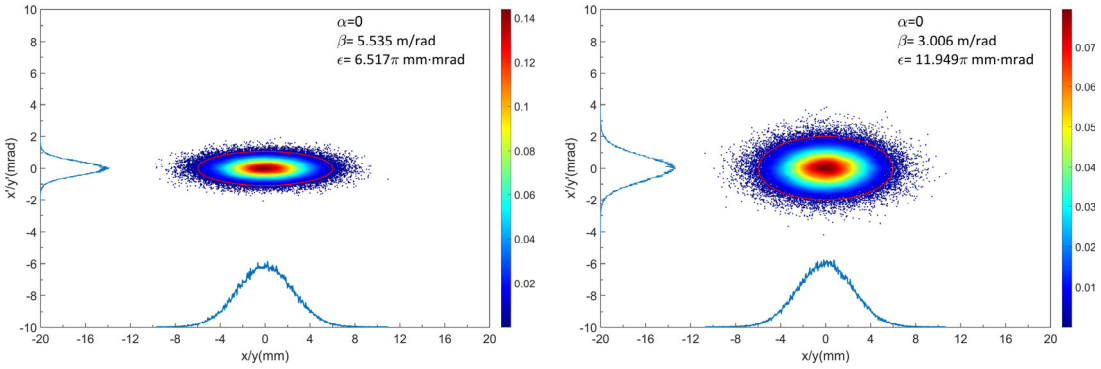

(a) (b)

Fig. 4. Particle distributions in transverse phase spaces for U beam (a) before stripping (b) after stripping. Emittance is 6-rms emittance.

The injection turn number for the stripped U beam is much lower than the designed value due to the unavoidable emittance growth during stripping. Comparing the phase space distributions before and after stripping, one can find that there is nearly no change in the beam envelope and that the emittance growth is completely dominated by the increase of the beam divergence. It is easy to understand: the stripper thickness is too thin to demonstrate the change of the particle transverse positions, while the angle straggling due to the small-angel scattering superposed on the initial beam angular spread makes the change of the beam divergence non-negligible. Thus, the angular spread and the emittance of the stripped beams can be calculated with the following analytic expressions.

$$\sigma_{x'(y')-f} = \sqrt{\sigma^2_{x'(y')-i} + \sigma^2_{sct-ang}} = \sqrt{\frac{\varepsilon_{x(y)-rms-i}}{\beta_{x(y)-i}} + \sigma^2_{sct-ang}} \tag{12}$$

$$\varepsilon_{x(y)-rms-f} = \sigma_{x(y)}\sigma_{x'(y')-f} = \sqrt{\varepsilon^2_{x(y)-rms-i} + \sigma^2_{x(y)}\sigma^2_{sct-ang}} \tag{13}$$

where $\varepsilon_{x(y)\text{-}rms}$ is the horizontal/vertical rms emittance; $\beta_{x(y)}$ is the horizontal/vertical beta function; $\sigma_{x(y)}$ and $\sigma_{x'(y')}$ are the horizontal/vertical rms beam size and the horizontal/vertical rms angular spread, respectively; the i and f in the subscripts denote the indexes for the beam before and after stripping, respectively, and $\sigma_{sct\text{-}ang}$ is the rms angle straggling of the ions introduced by the small-angle scatterings in the stripper. The holding of the second equality of Equation 12 was based on the precondition of the beam with upright beam ellipses in the transverse phase spaces, i.e., the transverse alpha functions α_x and α_y equaling 0. This is not just for convenience. More importantly, for a beam with fixed emittance and beam size, the emittance growth due to stripping gets to the minimum when the beam has upright ellipses in the transverse phase spaces [52]. The angle straggling $\sigma_{sct\text{-}ang}$ due to the small-angle scattering is correlated to the mass and energy of the projectile, the mass of the target atom, and the stripper thickness. It is irrelevant to the initial incident angle. It can be calculated by the codes SRIM or GEANT4, and it is 0.68 mrad for the U beam. Taking the value of $\sigma_{sct\text{-}ang}$ into Equation 13, one can get the rms emittance of 1.987 π mm·mrad after stripping for the U beam, consistent with the results presented in Fig. 4. The emittances after stripping were also calculated for the Xe and Kr beams with Equation 13 and GEANT4 as for the U beam presented in Fig. 4. The results by the two approaches also agree. The consistency confirms the validity of the formulae. From Equation 13, we can get an important conclusion that for a certain initial emittance, the larger the beam size on the stripper, the larger the emittance growth induced by stripping because the angle straggling due to the small-angle scatterings in the stripper is irrelevant to the initial beam emittance and envelope. Therefore, the number of injection turns can be enhanced by shrinking the beam size on the stripper.

Substituting Equation 13 into Equation 11, one can get the necessary beam pulse duration for injecting the stripped ions as follows.

$$\tau \approx \frac{1}{36}\alpha\tau_r \frac{A_x A_y}{\varepsilon_{x-rms-f}\varepsilon_{y-rms-f}} = \frac{1}{36}\alpha\tau_r \frac{A_x A_y}{\sqrt{\left(\varepsilon_{x-rms-i}^2+\sigma_x^2\sigma_{sct-ang}^2\right)\left(\varepsilon_{y-rms-i}^2+\sigma_y^2\sigma_{sct-ang}^2\right)}} \tag{14}$$

where τ is the necessary beam pulse duration, and τ_r is the revolution period for the ions considered. Taking the circumference of the BRing, 569 m, into account, the revolution period is 10.2, 7.69, and 8.08 μs for the stripped U, Xe, and Kr ions, respectively. The factor $\frac{1}{36}$ in Equation 14 was introduced because the beam emittances utilized here are the rms emittances. Although shrinking the beam size on the stripper can enhance the number of injection turns, it will also increase the stripper temperature because of the increasing particle density in one beam pulse. Therefore, caution must be paid when reducing the beam size because the stripper temperature will approach and even exceed the constraint at some beam sizes. If the beam size is further decreased beyond the critical point, with which the stripper temperature exceeds the temperature constraint, the current intensity must be reduced correspondingly. As discussed above, the energy deposited by the beam could be treated as instantaneous. Thus, the maximum foil temperature is positively correlated to the ion density at the beam center during one beam pulse, no matter how long the beam pulse duration is. That is to say, the maximum foil temperature could be kept under the constraint provided that the ion density was kept below a certain value. Therefore, the highest pulsed beam intensity tolerable for the foil is proportional to the beam size and inversely proportional to the beam pulse duration. Taking the expression of the necessary beam pulse duration, Equation 14, we can get the relationship between the highest tolerable beam intensity and the beam size expressed in a semi-quantitative form.

$$I_{max} \propto \sigma_x\sigma_y\sqrt{\varepsilon_{x-i}^2+\sigma_x^2\sigma_{sct-ang}^2}\sqrt{\varepsilon_{y-i}^2+\sigma_y^2\sigma_{sct-ang}^2} \tag{15}$$

Some factors are ignored in the above discussion, such as the dependence of the heat capacity and the heat conduction on the temperature, the change of the temperature gradient due to the change of the beam size, and the high-order terms in Equation 7. Nevertheless, the particle number injected into the ring can be estimated roughly by combining Equations 14 and 15.

$$N_{inj} = \kappa_{str}\frac{I_{max}}{q}\tau \propto \sigma_x\sigma_y \tag{16}$$

where κ_{str} is the stripping efficiency, which has been given in Section 3 for the typical ions. Now, based on Equations 11, 13, 15, and 16, the final emittance, the injection turn number, the highest tolerable beam intensity, and the number of the particles injected into the ring are plotted against the beam size for the U beam in Fig. 5 (a). With the plots, it is easy to find appropriate working points. The number of the injected ions increases with the beam size, although the injection turn number decreases because of the increased emittance. This is because the tolerable beam intensity increases with the beam size nearly quadratically, i.e., faster than the decreasing trend of the injection turn number. But it has to be mentioned that the beam intensity could not keep increasing with the beam size, and hence neither did the injected ion number, given the designed beam intensity of 1 emA. The beam size, with which the tolerable beam intensity gets to 1 emA, is indicated with the green dot-dash line in Fig. 5 (a). The trend of the injected ion number for the beam size beyond this critical point, provided that the beam intensity is kept at 1 emA, is presented with the dashed magenta line.

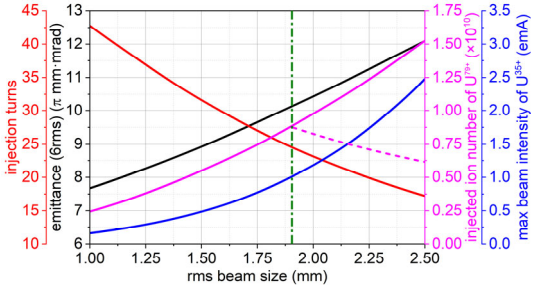

(a)

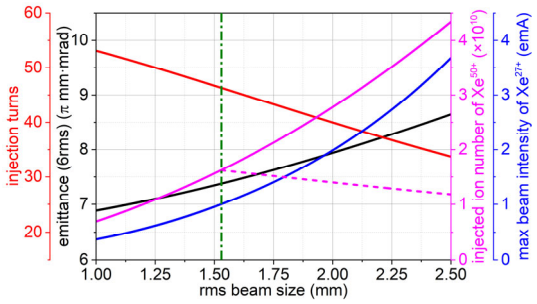

(b)

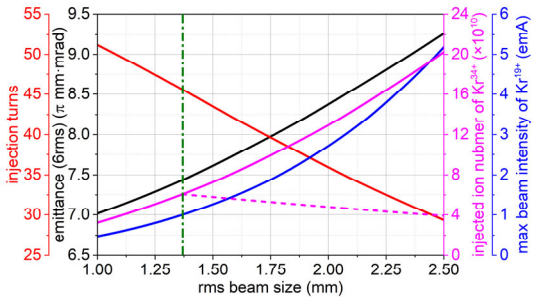

(c)

Fig. 5. Relationships between emittance after stripping (black solid lines), number of injection turns (red solid lines), highest tolerable beam intensity (blue solid lines), number of injected particles (magenta solid lines) and rms beam size: (a) for U beam, (b) for Xe beam and (c) for Kr beam. Green dot-dash lines indicate the beam size beyond which the highest tolerable beam intensity exceeds 1 emA, designed value for iLinac. Magenta dash lines present trend of injected ion number when input beam current is kept at 1 emA.

It must be emphasized that the plots in Fig. 5 are only utilized to quickly evaluate the working points: for a certain beam size, how much will the emittance be after stripping and how many stripped ions can be injected into the ring roughly? In calculating the injected particle number, the beam loss along the beamline from the stripper to the injection point and during the injection was not considered. Therefore, to get the accurate number of particles that can be accumulated in the ring, detailed simulation and optimization procedures, such as the work in Refs. [47] and [53], are needed.

Except for the accumulated ion number in the ring, the accurate foil temperature must also be calculated with the thermal analysis presented in Section 5.2. Here, we choose two beam sizes: one is the smallest size presented in Fig. 5, 1 mm, and the other is the beam size of 1.89 mm, with which the highest tolerable beam intensity achieves 1 emA. The temperature evolution at the hot spot simulated by Ansys for these two U beam sizes is presented in Fig. 6 (a) with their respective highest tolerable beam intensities indicated in the legends and the corresponding emittances after stripping, injection turn numbers, beam pulse durations, and injected particle numbers listed in Table 3. With the temperature evolution, the evaporation rate at the hot spot averaged over one second, i.e., the repetition period of the beam pulses, is 6×10^{-9} (μg/cm^2)/s for both beam sizes, because the temperature evolution in the two cases is the same. However, the peak temperature is slightly different.

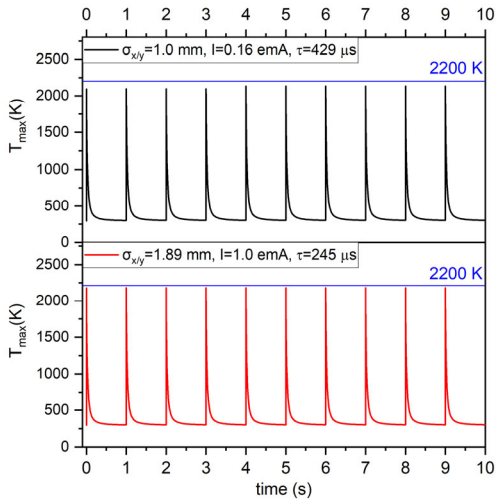

(a)

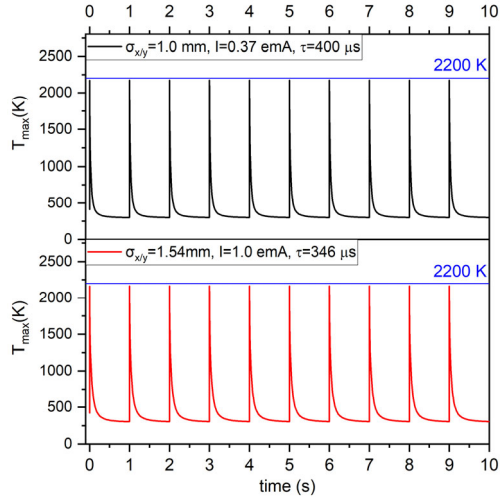

(b)

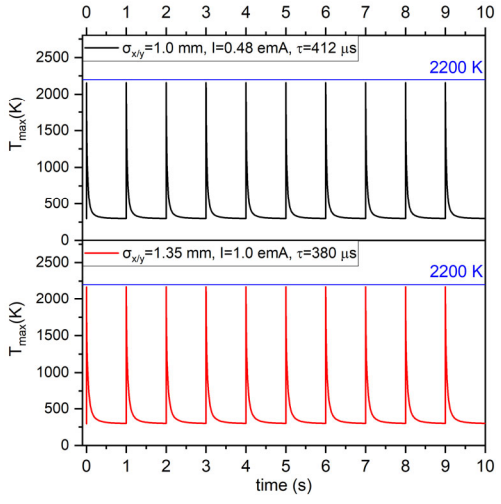

(c)

Fig. 6. Temperature evolution at hot spot simulated by Ansys: (a) for U beam size of 1 and 1.89 mm, (b) for Xe beam size of 1 and 1.54 mm, (c) for Kr beam size of 1 and 1.35 mm.

Similarly, the dependence of the corresponding parameters on the beam size was also derived for the Xe and Kr beams and plotted in Figs. 5 (b) and (c). The temperature evolution at the hot spot for two beam sizes for each ion species is presented in Figs. 6 (b) and (c). The corresponding parameters for these two beam sizes are listed in Table 3.

ion species	rms beam size (mm)	emittance after stripping (6rms) (π mm·mrad)	number of injection turns	beam pulse duration (μs)	average beam intensity on stripper (enA)	number of injected ions ($\times 10^{10}$)	maximum temperature (K)
U	1.0	7.67	42	429	69	0.24	2134.7
	1.89	10.10	24	245	245	0.86	2182
Xe	1.0	6.89	52	400	148	0.67	2175.8
	1.54	7.39	45	346	346	1.6	2164.7
Kr	1.0	6.96	51	412	198	3.2	2155.4
	1.35	7.28	47	380	380	6.2	2172.6

Table 3. Emittance after stripping, injection turn number, beam pulse duration, average beam intensity on stripper injected particle number, and maximum temperature for U, Xe, and Kr beams with different beam sizes

With the beam parameters in Table 3, the foil lifetime due to radiation damages calculated by LISE++ is 25.85, 622.35, and 2110.94 hrs for U, Xe and Kr beams. The results for the two beam sizes are the same because the averaged particle flux density is nearly the same in the two cases.

6. Summary and discussion

A C-foil stripper is planned to be utilized to strip ions to higher charge states at the injection beamline to the BRing when higher beam energy from the ring is desired. The key parameters of the stripped beams, such as the charge state distributions, the energy losses, and the energy distributions, were simulated for the typical heavy ion species. When a closed shell or subshell electron configuration is encountered during stripping, it will take extraordinary foil thickness to get the equilibrium charge state, causing excessive energy loss, energy straggling, and emittance growth. In this case, a much thinner foil thickness is adopted instead of equilibrium thickness as the choice for Xe and Kr beams. This results in higher stripping efficiency and much better beam quality on a tradeoff of only one or two lower charge states.

Except for the conflict between the stripped charge state and the stripping efficiency, there is a much more complicated situation involving foil temperature, emittance growth during stripping, and even the injection turn number of the ring. Simply put, the beam with a larger beam size is favorable considering the heating of the foil by the beam. In contrast, such a beam will suffer more considerable emittance growth due to stripping, and consequently, the injection turn number into the ring decreases dramatically. To work out a compromise between the lifetime of the foil and the number of injection turns, an analytic approach has been developed and can be utilized to evaluate all the parameters correlated to the beam size conveniently. Given the constraint on the foil temperature, 2200 K, and the designed beam intensity of the iLinac, 1 emA, the number of the injected ions into the ring is much smaller for stripped ions than that for unstripped ions, especially in the case of very heavy ions, owing to the lower stripping efficiency, the lower specific energy and the thicker stripper foil they need. For example, the number of the injected U^{79+} ions is lower by more than one order of magnitude compared with the number of the injected U^{35+} ions.

Because the emittance growth during stripping is non-negligible, elaborate calculations and optimization are needed to transport and inject the stripped ion beams. The results presented here can be utilized for these purposes.

Acknowledgments

This work is supported by the High-Intensity heavy-ion Accelerator Facility (HIAF) project approved by the National Development and Reform Commission of China.

References

[1] J. C. Yang, J. W. Xia, G. Q. Xiao et al., High Intensity heavy ion Accelerator Facility (HIAF) in China. Nucl. Instrum. Meth. B **317**, 263–265 (2013). https://doi.org/10.1016/j.nimb.2013.08.046

[2] H. W. Zhao, H. S. Xu, G.Q. Xiao et al., Huizhou accelerator complex facility and its future development. Sci. Sin.-Phys. Mech. Astron. **50**, 112006 (2020). https://doi.org/10.1360/SSPMA-2020-0248 (in Chinese)

[3] G. Q. Xiao, H. S. Xu, S. C. Wang, HIAF and CiADS National Research Facilities: Progress and Prospect. Nucl. Phys. Rev. **34**, 275-283 (2017). https://dx.doi.org/10.11804/NuclPhysRev.34.03.275 (in Chinese)

[4] X. H. Zhou, Physics Opportunities at the New Facility HIAF. Nuclear Physics Review **35**, 339-349 (2018). https://doi.org/10.11804/NuclPhysRev.35.04.339

[5] X. H. Zhou, J. C. Yang and the HIAF project team, Status of the high-intensity heavy-ion accelerator facility in China. AAPPS Bull. **32**, 35 (2022). https://doi.org/10.1007/s43673-022-00064-1

[6] H. W. Zhao, L. T. Sun, J. W. Guo et al., Superconducting ECR ion source: From 24-28 GHz SECRAL to 45 GHz fourth generation ECR. Rev. Sci. Instrum. **89**, 052301 (2018). https://doi.org/10.1063/1.5017479

[7] L. Sun, H. W. Zhao, H. Y. Zhao et al., Overview of high intensity ion source development in the past 20 years at IMP. Rev. Sci. Instrum. **91**, 023310 (2020). https://doi.org/10.1063/1.5129399

[8] L. Sun, W. Lu, H.W. Zhao et al., Progress on the development of key technologies for the fourth generation ECR ion source FECR. J. Phys.: Conf. Ser. **2244**, 012021 (2022). https://doi.org/10.1088/1742-6596/2244/1/012021

[9] Z. J. Wang, Y. He, H. Jia et al., Conceptual design of superconducting heavy ion linear injector for HIAF, in Proceedings of LINAC2012, 561–563 (2012). https://accelconf.web.cern.ch/LINAC2012/papers/tupb039.pdf

[10] Z. L. Zhang, X.B. Xu, Y. He et al., Design of a radio frequency quadrupole for a high intensity heavy-ion accelerator facility. Phys. Rev. Accel. Beams **25**, 080102 (2022). https://doi.org/10.1103/PhysRevAccelBeams.25.080102

[11] M.X. Xu, Y. He, S.X. Zhang et al., Low beta superconducting cavity system design for HIAF iLinac, Nucl. Eng. Technol. **55**, 2466-2476 (2023). https://doi.org/10.1016/j.net.2023.04.010

[12] L. J. Mao, J. C. Yang, J. W. Xia et al., Electron cooling system in the booster synchrotron of the HIAF project. Nucl. Instrum. Meth. A **786**, 91–96 (2015). https://doi.org/10.1016/j.nima.2015.03.052

[13] P. Li, Y. J. Yuan, J. C. Yang et al., The collimation system design for the Booster Ring in the HIAF project. Nucl. Instrum. Meth. A **920**, 14–21 (2019). https://doi.org/10.1016/j.nima.2018.12.064

[14] D. Y. Yin, J. Liu, G. D. Shen et al., Longitudinal Beam Dynamics for the Heavy-Ion Synchrotron Booster Ring at HIAF. Laser and Part. Beams **2021**, 6665132 (2021) https://doi.org/10.1155/2021/6665132

[15] L. N. Sheng, X. H. Zhang, J. Q. Zhang et al., Ion-optical design of High energy FRagment Separator (HFRS) at HIAF. Nucl. Instrum. Meth. B **439**, 1-9 (2020). https://doi.org/10.1016/j.nimb.2020.02.026

[16] B. Wu, J. C. Yang, J. W. Xia et al., The design of the Spectrometer Ring at the HIAF. Nucl. Instrum. Meth. A **881**, 27–35 (2018). https://doi.org/10.1016/j.nima.2017.08.017

[17] M.T. Tang, L.J. Mao, H.J. Lu et al., Design of an efficient collector for the HIAF electron cooling system. Nucl. Sci. Tech. **32**, 116 (2021). https://doi.org/10.1007/s41365-021-00949-0

[18] H. Okuno, N. Fukunishi, A. Goto et al., Low-Z gas stripper as an alternative to carbon foils for the acceleration of high-power uranium beams. Phys. Rev. ST Accel. Beams **14**, 033503 (2011). https://doi.org/10.1103/PhysRevSTAB.14.033503

[19] H. Imao, H. Okuno, H. Kuboki et al., Charge stripping of ^{238}U ion beam by helium gas stripper. Phys. Rev. ST Accel. Beams **15**, 123501 (2012). https://doi.org/10.1103/PhysRevSTAB.15.123501

[20] H. Hasebe, H. Okuno, A. Tatami et al., Development of a rotating graphite carbon disk stripper. AIP Conference Proceedings **1962**, 030004 (2018). https://doi.org/10.1063/1.5035521

[21] H. Hasebe, H. Okuno, A. Tatami et al., Development of a high-density highly oriented graphite stripper. EPJ Web Conf. **229**, 01004 (2020). https://doi.org/10.1051/epjconf/202022901004

[22] W. Barth, A. Adonin, C. E. Düllmann et al., U^{28+}-intensity record applying a H_2-gas stripper cell. Phys. Rev. ST Accel. Beams **18**, 040101 (2015). https://doi.org/10.1103/PhysRevSTAB.18.040101

[23] W. Barth, A. Adonin, Ch. E. Düllmann et al., High brilliance uranium beams for the GSI FAIR. Phys. Rev. Accel. Beams **20**, 050101 (2017). https://doi.org/10.1103/PhysRevAccelBeams.20.050101

[24] W. Barth, U. Scheeler, H. Vormann et al., High brilliance beam investigations at the universal linear accelerator. Phys. Rev. Accel. Beams **25**, 040101 (2022). https://doi.org/10.1103/PhysRevAccelBeams.25.040101

[25] F. Marti, P. Guetschow, Y. Momozaki et al., Development of a liquid lithium charge stripper for FRIB. Proceedings of HIAT2015, Yokohama, Japan, **TUA1I01**, 134–138 (2015). https://doi.org/10.18429/JACoW-HIAT2015-TUA1I01

[26] T. Kanemura, M. LaVere, R. Madendorp et al., Experimental demonstration of the thin-film liquid-metal jet as a charge stripper. Phys. Rev. Lett. **128**, 212301 (2022). https://doi.org/10.1103/PhysRevLett.128.212301

[27] H. D. Betz, Charge states and charge-changing cross sections of fast heavy ions penetrating through gaseous and solid media. Rev. Mod. Phys. **44**, 465–539 (1972). https://doi.org/10.1103/RevModPhys.44.465

[28] A. B. Wittkower and H. D. Betz, Equilibrium-charge-state distributions of energetic ions (Z>2) in gaseous and solid media. Atomic Date **5**, 11–166 (1973). https://doi.org/10.1016/S0092-640X(73)80001-4

[29] J. P. Rozet, C. Stéphan, D. Vernhet, ETACHA: a program for calculating charge states at GANIL energies. Nucl. Instrum. Meth. B **107**, 67–70 (1996). https://doi.org/10.1016/0168-583X(95)00800-4

[30] E. Lamour, P. D. Fainstein, M. Galassi et al., Extension of charge-state-distribution calculations for ion-solid collisions towards low velocities and many-electron ions. Phys. Rev. A **92**, 042703 (2015). https://doi.org/10.1103/PhysRevA.92.042703

[31] E. Baron, M. Bajard and Ch. Ricaud, Charge exchange of very heavy ions in carbon foils and in the residual gas of GANIL cyclotrons. Nucl. Instrum. Meth. A **328**, 177–182 (2015). https://doi.org/10.1016/0168-9002(93)90622-O

[32] S. Ouichaoui and B. Bouzid, Energy loss straggling of swift heavy ions below 100 MeV/u. Nucl. Instrum. Meth. B **193**, 36–42 (2002). https://doi.org/10.1016/S0168-583X(02)00724-3

[33] S. Agostinelli, J. Allison, K. Amako et al., GEANT4—a simulation toolkit. Nucl. Instrum. Methods Phys. Res. A **506**, 250–303 (2003). https://doi.org/10.1016/S0168-9002(03)01368-8

[34] J. Allison, K. Amako, J. Apostolakis et al., Recent developments in GEANT4. Nucl. Instrum. Meth. A **835**, 186–225 (2016). https://doi.org/10.1016/j.nima.2016.06.125

[35] J. F. Ziegler, M. D. Ziegler, J. P. Biersack, SRIM – The stopping and range of ions in matter (2010). Nucl. Instrum. Meth. B **268**, 1818–1823 (2010). https://doi.org/10.1016/j.nimb.2010.02.091

[36] C. Scheidenberger, H. Geisse, H. H. Mikkelsen et al., Energy-Loss-Straggling Experiments with Relativistic Heavy Ions in Solids. Phys. Rev. Lett. **77**, 3987 (1996). https://doi.org/10.1103/PhysRevLett.77.3987

[37] B. Efken, D. Hahn, D. Hilscher et al., Energy loss and energy loss straggling of N, Ne, and Ar ions in thin targets. Nucl. Instrum. Meth. **129**, 219-225 (1975). https://doi.org/10.1016/0029-554X(75)90132-9

[38] P. Sigmund, O. Osmani and A. Schinner, Charge-exchange straggling in equilibrium. Nucl. Instrum. Meth. B **269**, 804–809 (2011). https://doi.org/10.1016/j.nimb.2010.11.094

[39] Q. Yang, D. J. O'Connor, Z. L. Wang, Empirical formulae for energy loss straggling of ions in matter. Nucl. Instrum. Meth. B **61**, 149-155 (1991). https://doi.org/10.1016/0168-583X(91)95454-L

[40] N. Bohr, XXII. The penetration of atomic particles through matter, Niels Bohr Collected Works **8**, 423-568 (1987); Original publication in: Mat. Fys. Medd. K. Dan. Vidensk. Selsk. **18**, (1948). https://doi.org/10.1016/S1876-0503(08)70172-5

[41] W. K. Chu, Calculation of energy straggling for protons and helium ions. Phys. Rev. A **13**, 2057 (1976). https://doi.org/10.1103/PhysRevA.13.2057

[42] S. G. Lebedev and A. S. Lebedev, Calculation of the lifetimes of thin stripper targets under bombardment of intense pulsed ions. Phys. Rev. ST Accel. Beams **11**, 020401 (2008). https://doi.org/10.1103/PhysRevSTAB.11.020401

[43] LISE++ (Version 16.15.17). https://lise.nscl.msu.edu/lise.html

[44] S. A. Miller, C. S. Jolivet, J. O. Stoner Jr., New methods for testing cyclotron carbon stripper foils. Nucl. Instrum. Meth. A **590**, 57–65 (2008). https://doi.org/10.1016/j.nima.2008.02.068

[45] A. L. Marshall and F. J. Norton, Carbon vapor pressure and heat of vaporization. J. Am. Chem. Soc. **72**, 2166–2171 (1950). https://doi.org/10.1021/ja01161a081

[46] C. J. Liaw, Y. Y. Lee, J. Alessi et al., Calculation of the maximum temperature on the carbon stripping foil of the Spallation Neutron Source. Proceedings of the 1999 Particle Accelerator Conference, New York, **5**, 3300–3302 (1999). https://doi.org/10.1109/PAC.1999.792283

[47] G. F. Qu, W. P. Chai, J. W. Xia et al., Two-plane painting injection scheme for BRing of HIAF. Nucl. Sci. Tech. **28**, 114 (2017). https://doi.org/10.1007/s41365-017-0260-5

[48] G. F. Qu, J. W. Xia, J. C. Yang et al., Simulation of Two Planes Painting Injection for HIAF-Bring. Nuclear Physics Review **35**, 28-33 (2018). https://doi.org/10.11804/NuclPhysRev.35.01.028

[49] C. R. Prior, G. H. Rees, Multiturn injection and lattice design for HIDIF. Nucl. Instrum. Meth. A **415**, 357-362 (1998). https://doi.org/10.1016/S0168-9002(98)00406-9

[50] R. W. Hasse, I. Hofmann, Space-charge limits of multiturn injection in HIDIF. Nucl. Instrum. Meth. A **415**, 478–483 (1998). https://doi.org/10.1016/S0168-9002(98)00517-8

[51] A. W. Chao, K. H. Mess, M. Tigner, F. Zimmermann (ed.), *Handbook of Accelerator Physics and Engineering,* 2nd Edition, (World Scientific, Singapore, 2013), p. 383.

[52] J. G. Hwang, E. S. Kim, H. J. Kim et al., Minimization of the emittance growth of multi-charge particle beams in the charge stripping section of RAON. Nucl. Instrum. Meth. A **767**, 153–158 (2014). https://doi.org/10.1016/j.nima.2014.08.018

[53] L. P. Yao, W. P. Chai, J. C. Yang et al., Beam-loss driven injection optimization for HIAF-BRing in the presence of space charge. Nucl. Instrum. Meth. A **951**, 162876 (2020). https://doi.org/10.1016/j.nima.2019.162876